AIP | Review of Scientific Instruments

Background-free imaging of plasmonic structures with cross-polarized apertureless scanning near-field optical microscopy

M. Esslinger, J. Dorfmüller, W. Khunsin, R. Vogelgesang, and K. Kern

Citation: Rev. Sci. Instrum. **83**, 033704 (2012); doi: 10.1063/1.3693346
View online: http://dx.doi.org/10.1063/1.3693346
View Table of Contents: http://rsi.aip.org/resource/1/RSINAK/v83/i3
Published by the American Institute of Physics.

Related Articles

Apertureless near-field microscopy using a knife blade as a scanning probe at millimeter wavelengths
J. Appl. Phys. 112, 074907 (2012)

Note: Quasi-real-time analysis of dynamic near field scattering data using a graphics processing unit
Rev. Sci. Instrum. 83, 106101 (2012)

Sensitivity maximized near-field scanning optical microscope with dithering sample stage
Rev. Sci. Instrum. 83, 093710 (2012)

Instrumentation for dual-probe scanning near-field optical microscopy
Rev. Sci. Instrum. 83, 083709 (2012)

Quantitative coherent scattering spectra in apertureless terahertz pulse near-field microscopes
Appl. Phys. Lett. 101, 011109 (2012)

Additional information on Rev. Sci. Instrum.

Journal Homepage: http://rsi.aip.org
Journal Information: http://rsi.aip.org/about/about_the_journal
Top downloads: http://rsi.aip.org/features/most_downloaded
Information for Authors: http://rsi.aip.org/authors

ADVERTISEMENT

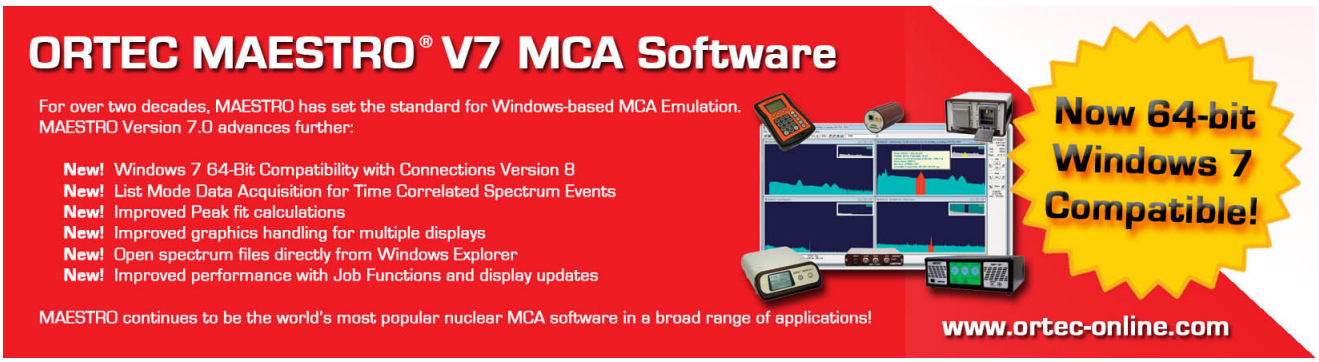

Background-free imaging of plasmonic structures with cross-polarized apertureless scanning near-field optical microscopy

M. Esslinger,[1,a)] J. Dorfmüller,[1,b)] W. Khunsin,[1] R. Vogelgesang,[1] and K. Kern[1,2]
[1]*Max-Planck-Institut für Festkörperforschung, 70569 Stuttgart, Germany*
[2]*Institut de Physique de la Matière Condensée, École Polytechnique Fédérale de Lausanne, 1015 Lausanne, Switzerland*

(Received 26 May 2011; accepted 22 February 2012; published online 15 March 2012)

We present advances in experimental techniques of apertureless scanning near-field optical microscopy (aSNOM). The rational alignment procedure we outline is based upon a phase singularity that occurs while scanning polarizers around the nominal cross-polarized configuration of s-polarized excitation and p-polarized detection. We discuss the theoretical origin of this topological feature of the setup, which is robust against small deviations, such as minor tip misalignment or shape variations. Setting the polarizers to this singular configuration point eliminates all background signal, allowing for reproducible plasmonic eigenmode mapping with optimal signal-to-noise ratio.
 [http://dx.doi.org/10.1063/1.3693346]

I. INTRODUCTION

In apertureless scanning near-field optical microscopy (aSNOM) deep subwavelength spatial resolution is achieved, for example, in imaging of local dielectric constant[1] or near-field distributions of plasmonic samples.[2,3] Often, a metallic tip is used as the local probe, which interacts strongly with the sample, resulting in detectable far-field scattering of high intensity. For dielectric samples, with an appropriate model for the tip-sample interaction, one can obtain local dielectric constant contrast at a sample surface, i.e., maps of the material composition.[4]

For plasmonic structures, however, maps of the local field distribution are at the center of interest. Unfortunately, such samples may themselves exhibit resonant eigenmodes, leading to non-trivial mode hybridization effects between the tip and the sample.[5] This coupling strongly influences the resulting images.[6–9] Their successful interpretation is typically not feasible without independent additional information about tip and sample. Usually, it also requires extensive simulations as there appears to be no general analytical model for this strong interaction case.

One way towards interpretable near-field images is the use of special, extremely weakly interacting probes, like carbon nanotube tips,[10] with correspondingly small detected signals. An interesting alternative is the predominant excitation of the sample, avoiding strong direct excitation of the probe—at least in the gap volume between probe and sample, where the local near-field signal is generated. In such a case the sample may indirectly, via near-field interaction, excite a suitable probe tip of significant scattering cross section. The scattered radiation is sufficiently intense to be easily detectable in the far-field and carries information mostly about the sample. This is the basic concept of the cross-polarization scheme for aSNOM.[3] In the idealized description, the illuminating beam is s-polarized, perpendicular to the tip axis. The detected radiation is analyzed for p-polarization, resulting from the local excitation of the tip by the sample.

Still, aSNOM is often plagued by background signal originating from imperfect alignment, which might even obscure any signal carrying information from the near-field region. Under favorable circumstances it is possible to clean up recorded data by numerical postprocessing, but the resulting near-field images are usually of inferior quality. In order to achieve highest signal-to-noise ratios (SNR), a systematic approach is much desired to eliminate this background already at the time of recording.

Several groups have presented results obtained in cross-polarization configuration[3,11,12] and discussed them in the vein of the above remarks. Here, we concentrate on the instrumentation and procedural aspects that facilitate the optimal alignment of aSNOM. We achieve nearly perfect background suppression using a topological singularity in the polarization phase space. Our rational alignment procedure results in routine, direct measurements of nearly unperturbed plasmonic eigenmodes with excellent quality.

II. SETUP

A detailed description of the main parts of our setup can be found in Ref. 13. It is based on a commercial atomic force microscope (AFM, M5 Park Scientific). After a short review of standard aSNOM instrumentation techniques we employ, we give a detailed description of our implementation of a cross-polarization scheme.

It is well known that a modulation–demodulation scheme facilitates the discrimination of near-field signal against parasitic background signals:[1,14] to this end, a lock-in amplifier is locked to the AFM cantilever deflection signal. Filtering the optical signal at a suitable harmonic of this frequency efficiently extracts the (spatially non-linear) near-field contributions. Care has to be taken that no mechanical anharmonicities are present.[15,16]

[a)]Electronic mail: m.esslinger@fkf.mpg.de.
[b)]Present address: 4. Physikalisches Institut, Universität Stuttgart, 70550 Stuttgart, Germany.

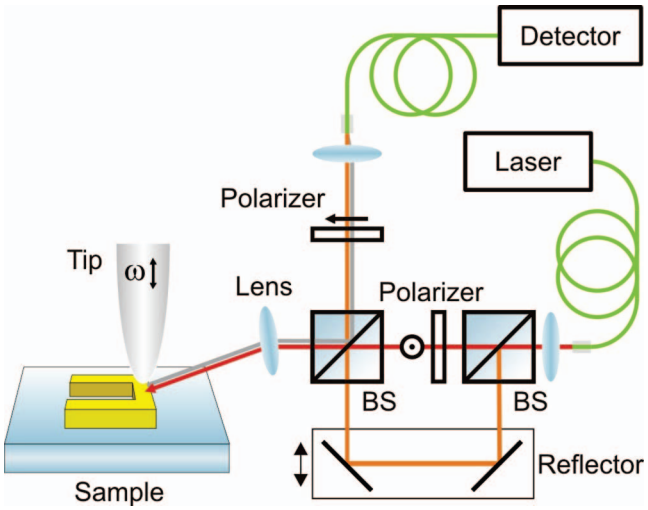

FIG. 1. Scheme of the setup. Focused s-polarized radiation excites the sample. Backscattered light is modulated by the tip vibration, polarization-analyzed in a cross-polarization scheme, and interferometrically amplified before it is sent to a detector. The beamsplitters (BS) form a Mach-Zehnder type of interferometer.

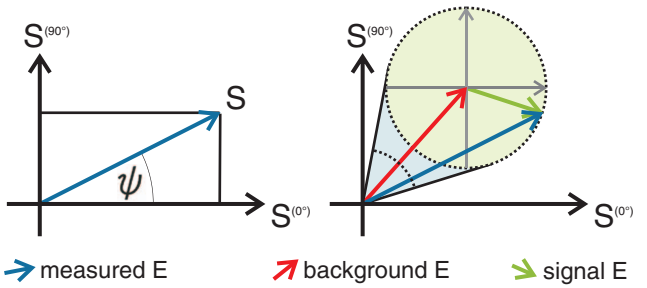

FIG. 2. A homodyne measurement consists of two values taken at different interferometric path differences. From those values, the complex-valued signal can be reconstructed. A large, constant background (red) overlaying the signal (green) will result in a limited phase range of the measured signal (blue). Under these circumstances, signals of equal magnitude and opposite phase can correspond to measured fields of different amplitude and similar phase.

In addition to the setup described in Ref. 13, we use a confocal arrangement for the optical microscopic detection path, where radiation is collected only from the diffraction limited image volume of a spatial filter centered at the tip apex. Single mode optical fibers (Thorlabs 780HP) provide convenient apertures[17–19] for both delivering light from the laser source to the setup as well as from the setup to the detector (see Figure 1).

The combination of filtering techniques introduced above significantly reduces the total signal intensity. The intensity of the illumination beam is limited by the damage threshold of the tip to about 0.5 MW/cm^2. This limits the intensity of the light scattered back from the near-field region onto the detector. Additionally, the detector and amplifier bandwidths have to be higher than the AFM cantilever frequency and its higher harmonics. Signal strengths are often hardly above the noise level of typical high-bandwidth, linear detectors. A standard way to overcome this is an optical amplification scheme.[1] The weak signal carrying beam is interferometrically amplified with a stronger reference beam.[20] Once the signal is amplified well above the noise level of the detector-amplifier system, no further improvement of the SNR is possible.[21–23] We use a Mach-Zehnder-type interferometric amplification scheme (see Figure 1). After splitting off the reference beam, a Glan-Taylor prism polarizes the excitation beam to the s-state. A second polarizer selects the p-component of the superimposed beams behind the combining beam splitter. With motorized rotation stages for the two Glan-Taylor prisms we can scan the polarizations systematically to find the optimal configuration.

Interferometric amplification also allows extracting both the amplitude and relative phase between signal and reference beam. Over the years several schemes have been employed in aSNOM, in close analogy to information encoding techniques in signal processing electronics.[18,20,24–26]

In our instruments we use a homodyne scheme. Amplitude and phase are reconstructed from two measurements S_1 and S_2 with a phase difference of the reference path of $+90°$. Both measurements are projections of the complex-valued total signal S on two lines with – in our case – an angle difference of 90° in the complex plane (see Figure 2). Total amplitude and optical phase ψ can be calculated by

$$S = \sqrt{S_1^2 + S_2^2}, \tag{1}$$

$$\tan\psi = \frac{S_2}{S_1}. \tag{2}$$

To be able to address the full range of $\psi \in [0, 360°)$, it is crucial to attribute a sign to the two measured amplitudes $S_{1,2}$, in order to obtain a proper optical phase that coincides with numerical calculations.[3] One way is to assign a negative amplitude whenever the lock-in detector phase (available range $-180°$ to $+180°$) is below zero and positive otherwise. From the two signs of $S_{1,2}$ the value of ψ is thus fixed uniquely.

In the cross-polarization scheme the exciting and detected field components are orthogonally polarized.[3,27,28] Using s-polarized light for illumination, the tip is hardly excited at all.[29] In contrast, the structures on the sample may respond to s-polarized excitation with strong plasmonic resonances. The tip efficiently picks up the local vertical field components of these resonances and scatters them back into the far-field as mainly p-polarized light. We place a second polarizer in front of the detector, set to p-polarization.

Regarding the interferometric signal amplification the different types of interferometers demand different implementations. In a Michelson type interferometer the light is polarized to ensure s-polarization in the illumination path. By including a λ/4-plate in the reference arm the polarization is turned by 90° and only the p-polarized component of the scattered light is amplified.[11] We view a Mach-Zehnder interferometer as preferable since it allows an independent manipulation of the two partial beams, offering direct, full control of the polarization states in both paths. After splitting off the reference beam, a Glan-Taylor prism polarizes the illumination to the s-state. The scattered light is mixed with the reference

beam in a second beam splitter, and a second polarizer selects the p-component of both beams.

We use non-contact AFM tips (Nanosensors, AdvancedTEC NC) made of silicon.[6,13] To our experience, this kind of probe provides sufficient scattering cross section with little or no parasitic coupling. For plasmonic resonant gold structures in the visible to near-infrared region, we do not observe perturbations of the sample compared to FDTD calculations not including the silicon tip.[3] For more delicate systems, more weakly interacting tips could be necessary.

III. ALIGNMENT AND VERIFICATION

Having situated the tip at the center of the three-dimensional focal volume, one usually finds a finite backscattering background in the cross-polarized detection channel. Without further optimization, this is essentially an unavoidable consequence of a variety of experimental imperfections: AFM tips are not suitably shaped and aligned, the illumination is not a properly Gaussian beam, etc. The next alignment step is therefore to examine whether optimal cross polarization can be established by optimizing the polarizer settings. In our experience, it is usually possible to find polarizer settings, which show *zero* backscattering intensity.

The optimal configuration is indicated by the occurrence of a phase singularity in the backscattered radiation when scanning the polarizers. The theoretical background of this singularity will be explained below. To locate it experimentally, we need to use interferometry to gain phase sensitivity, recording the homodyne amplitude and phase. The systematic search then involves raster-scanning the two linear polarizers each by a few degrees around the nominal alignment. A typical two-dimensional data set that results from such a scan in polarization parameter space is shown in Figure 3.

The position 0°/90° for both polarizers marks the position of nominal cross polarization. The actual minimum we find in the amplitude scan is at a slightly different position. An indication what the optimal setting can be is found in the corresponding phase image. Encircling the lowest intensity pixel, a phase accumulation of 2π becomes evident – the classic signature of a topologically non-trivial feature. The implied phase singularity associated with this minimum is thus

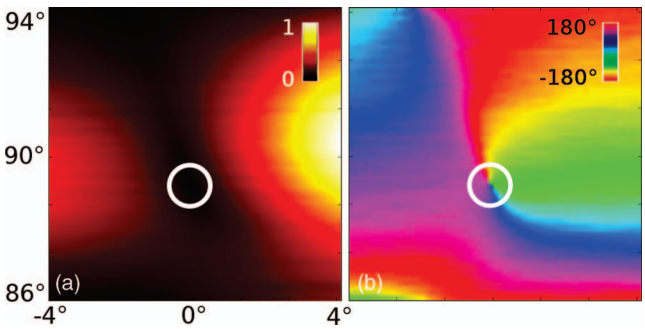

FIG. 3. Systematic search for the ideal polarizer angles. Illumination (horizontal axis) and detection (vertical axis) polarizer are scanned around the nominal cross-polarization position 0°/90°. The images show measurements of (a) the optical amplitude in arbitrary units and (b) the optical phase. The position of the phase singularity is marked in both images.

a mathematical *point* in parameter space. Barring the usual experimental caveats, such as accuracy in parameter setting, measurement noise, or stability, the background signal can be set not only below the detector noise, but to actual zero level. In our setup, this minimum is typically found at polarizer positions within ±5° off the nominal position.

IV. THE NATURE OF THE PHASE SINGULARITY

The occurrence of a phase singularity in the polarizer scans described above is a natural consequence of two orthogonal tip modes being excited. As they are excited and recorded in the far-field with two orthogonally polarized modes (s- and p-polarization), it is convenient to employ the Jones formalism to describe the detected signal. Scattering from the tip apex region – when properly centered in a Gaussian focus – is well approximated by a polarization ellipsoid.[4,14,29] It responds to excitation by s- and p-polarized light with two orthogonal modes (see also Figure 4).

The symmetry of this idealized system causes radiation emitted by the excited tip to be again linearly polarized in the same modes as the excitation radiation. Hence, off-diagonal elements of the Jones matrix describing the tip backscattering are zero,

$$\mathrm{T} = \begin{pmatrix} \alpha_s & 0 \\ 0 & \alpha_p \end{pmatrix}, \tag{3}$$

where $\alpha_{s,p}$ are complex-valued coefficients describing the backscattering strength of the tip due to the two modes. The linear polarizers used in the excitation and detection paths are described by

$$\mathrm{P}(\theta) = \begin{pmatrix} \cos(\theta)\cos(\theta) & \cos(\theta)\sin(\theta) \\ \sin(\theta)\cos(\theta) & \sin(\theta)\sin(\theta) \end{pmatrix}. \tag{4}$$

The detected signal after passage through the whole system, with the two polarizers at angles $\theta_{in,\,out}$, reads

$$\mathbf{E}_{out} = \mathrm{P}(\theta_{out}) \cdot \mathrm{T} \cdot \mathrm{P}(\theta_{in}) \cdot \mathbf{E}_{in}. \tag{5}$$

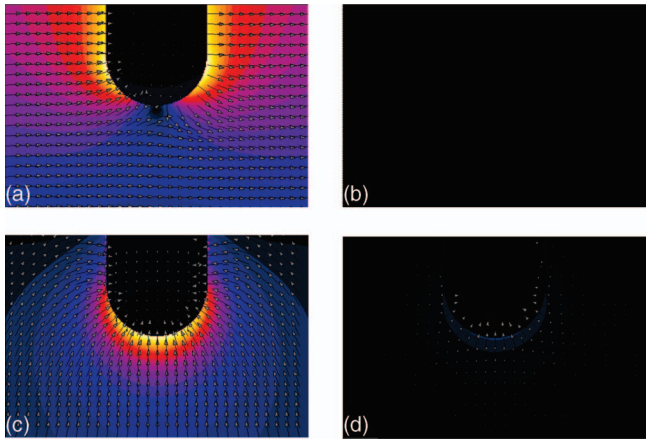

FIG. 4. Simulated near-fields at one end of a gold nanorod, excited by linearly polarized light of 900 nm wavelength. The apex radius is 30 nm, field of view is 180 nm × 120 nm. (a) and (b) real and imaginary part of the electric field for horizontally polarized excitation (s-polarized). (c) and (d) real and imaginary part of the electric field for vertically polarized excitation (p-polarized).

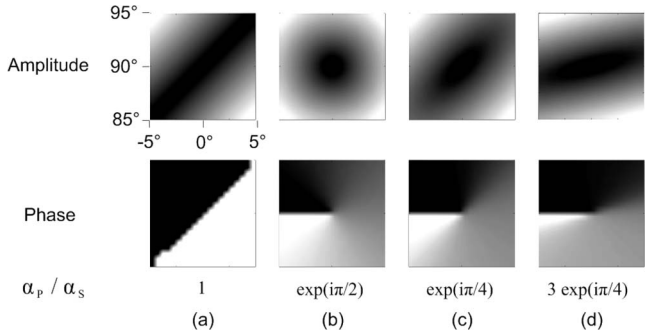

FIG. 5. Simulations of cross-polarization scans using Eq. (5). (a) When both modes of the tip $\alpha_{s,p}$ are degenerate, no singularity in phase is observed. Arbitrary phase differences other than $0,\pi$ lead to the occurrence of phase singularities in the cross-polarization position. The special case of $\alpha_p = \exp(i\pi/2)\alpha_s$, as displayed in (b), yields a perfectly round minimum. Different retardations (c) and strengths (d) of both modes lead to an elongated elliptical minimum.

Typical examples for signal strengths simulated with Eq. (5) for different polarizer angles and polarizabilities are illustrated in Figure 5. Generally, a phase singularity is observed located at the nominal cross-polarization position. The amplitude images exhibit an elliptical shape, whose orientation and eccentricity depend on both the relative magnitudes and phases of α_s and α_p. Only for the degenerate case of a relative phase difference between the two polarizabilities of zero or 180° does the phase singularity become a line of zero amplitude.

In passing we note the possibility to extract from such scans – with corresponding analysis, based on Eq. (5) – the complex-valued ratio α_p / α_s. That is, the relative dipolar polarizabilities of an unknown tip can be characterized. In this sense, our polarizer scans are related to particle tip characterizations employed in previous studies.[30,31]

In a real setup, the perfect symmetry stipulated above is not realized. However, the presence of a phase singularity is a *topological property* of the system. As such it is quite robust against small, continuous deviations. For example, small rotations or displacement of the tip in space – being adiabatic evolutions of the system – do not abruptly destroy the phase singularity. Slight adjustments to the polarizer angles allow it to be recovered.

Similar arguments hold for adiabatic deformations of the tip. These introduce small, non-dipolar polarizabilities, whose backscattering is superimposed on the dipolar response. Still, for not too large deformations, it is possible to find cross polarization. By slightly realigning the polarizers the coherent superposition of dipolar and (small) non-dipolar scattering is such that an exact linearly polarized state is formed at the second polarizer.

It takes more drastic deviations from the presumed perfectly conical tip shape to develop sufficiently strong non-dipolar polarizabilities that always lead to some non-linearly polarized backscattered signal, regardless of input polarizer alignment. In this case, no phase singularity is observed in the polarizer scans, only a finite minimum amplitude. On the one hand, this forces us to reject some of the commercial AFM tips we employ (less than 40%). On the other hand, the systematic cross polarization scan thus provides a welcome rational method for screening the suitability of AFM tips for aSNOM.

V. APPLICATIONS

After aligning the setup we approach the sample from below until it is in proximity of the tip. Keeping the tip fixed in space, we raster scan the sample with a piezo stage (Physik Instrumente P-517.3CD). From the AFM feedback loop and optical signal we obtain images of the topography as well as optical amplitude and phase. Figures 6(a)–6(c) show an image taken with an imperfect cross-polarization alignment. The topography image shows gold discs on a SiO_2 substrate. Detailed studies of such structures have been published earlier.[3,32] In the optical image the dipolar character is visible as one bright and one dark lobe compared to the regions in between the discs. At the same time the phase image shows contrast only in a few regions. The areas where the phase deviates from the otherwise uniform rest correspond to the dark areas of the amplitude image.

We explain these observations by assuming an additional background signal overlaying our optical near-field signal (see Figure 2). Light being backscattered by solely the tip or solely the sample leads to a nonzero background. To our experience, this background is mostly constant or drifts linearly in time. One may evaluate the complex-valued signal in an area between the structures, where very small signal amplitudes are expected. By subtracting this complex-valued background we obtain a new amplitude and phase signal

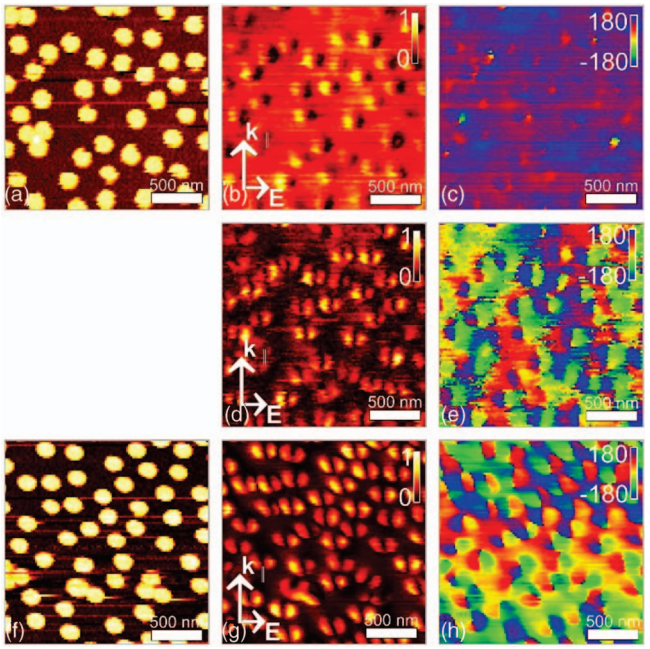

FIG. 6. (a) AFM topography of gold discs on silicon dioxide substrate illuminated with (b) and (c) optical amplitude and phase of those discs with nonzero background. (d) and (e) Optical amplitude and phase after subtraction of constant complex background. (f) AFM topography of a different region on the same sample after realignment of the setup. (g) and (h) Optical amplitude and phase of the discs shown in (f). Background is lower than in the previous measurement, making background subtraction unnecessary.

which is now nearly zero over the whole background region. The amplitude image, postprocessed in this fashion, (Figures 6(d) and 6(e)) shows two bright lobes on the dipole discs and the phase difference of both lobes is close to 180°.

Rather than by postprocessing, it is desirable to eliminate the background signal already at the time of recording by establishing cross polarization. Figures 6(f)–6(h) show the raw data obtained from the same sample after realigning the setup to exact cross polarization. A comparison shows clearly the improved signal-to-noise ratio, thanks to the cross-polarization alignment.

The cross-polarized aSNOM technique can also be used to obtain faithful near-field information from rather complex plasmonic structures. Here we discuss the example of linear feed-gap antennas consisting of two gold wires fabricated by electron beam lithography. Fabrication and size parameters are systematically varied to tune the resonance frequencies and identify optimal structures with the desired optical response. To demonstrate the potential of cross polarization, we measure different configurations of illuminating and scattered beams.

Figure 7(a) shows the images measured in cross polarization. With the electric field of the incident beam in the direction of the wire, the antennas are strongly excited. In this configuration, lobes of the electric field strength are observed on the resonant wires. The plasmonic eigenmodes are mostly unperturbed.[3] Background signal in regions without metallic structures is low. When we place the antennas perpendicular to the incident electric field (Figure 7(b)), we excite transverse modes of the wire. These do not depend on the wire length, only on its width. The structures are not resonant for this mode.

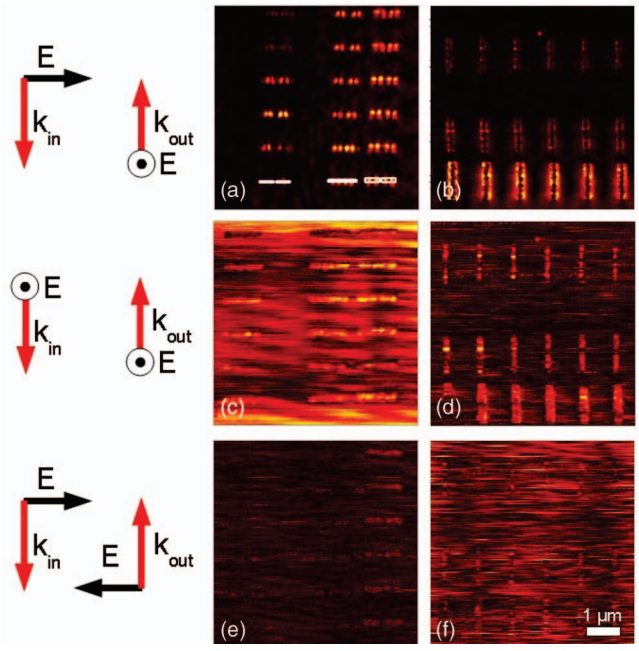

FIG. 7. Near-field images of feed-gap antennas under different illumination conditions at $\lambda = 911$ nm. The antennas are made of gold on a silicon dioxide substrate. (a) and (b) Cross-polarization scheme. In (a), the topography of the lowest row is marked in white. From the left to the right, the wire thickness varies. From top to bottom, the gap size changes. In (b), the sample is rotated in the image plane by 90°. Non-resonant transversal modes are excited. (c) and (d) Both illumination and detection polarizers are aligned to p-polarization. (e) and (f) Both polarizers are aligned to s-polarization.

Using p-polarized for incident as well as detected light, both tip and sample are directly excited, couple to each other, and scatter back (see Figures 7(c) and 7(d)). Much of the contrast observed here stems from variations in the backscattering cross section of the coupled tip-sample system, which in turn largely depends on sample material. By comparing with simulations or a model,[12] one can gain information about the dielectric constant of the sample or even its dielectric tensor.[33]

When aligning both illumination and detection path to s-polarization, we obtain very low signal intensities in the near-infrared (see Figures 7(e) and 7(f)). Evidently, the tip cannot be efficiently excited by the incident beam, nor can it radiate efficiently with this polarization. In the mid-IR, for cases of particularly strong near-fields at a sample, such a configuration has been shown to allow mapping of in-plane components.[12]

VI. SUMMARY AND OUTLOOK

Filtering techniques and systematic alignment of an aSNOM in cross polarization can lead to background-free optical near-field images. We build upon the well-established techniques of higher harmonic demodulation for discrimination of near-field signal against background scattering and homodyne interferometric amplification for increased signal strength and access to the complex optical amplitude. In addition, we recommend a confocal optical setup for further increased background reduction and the use of spatial filtering for optimal interferometric visibility.

The main message, though, is the high-fidelity of near-field optical microscopy afforded by the cross-polarization scheme. We outline its systematic alignment, which leads to largely decoupled illumination and detection with very little perturbation of plasmonic sample eigenmodes. With the sample retracted, the alignment procedure routinely achieves background levels below the detector noise. With the sample in contact, all signal can thus be ascribed to tip-mediated scattering of local near-fields from the sample. Earlier[3] we showed that signals measured in cross polarization reproduce very well the vertical component of the electric field of the excited bare sample – as simulated in the absence of any probe tip.

As an outlook, one may consider a deliberate tilt of the probe tip with respect to the surface normal. A correspondingly rotated cross-polarization scheme can be envisioned, using polarization states compatible with such a tip. It may be expected to allow similarly background-free measurements of slanted field components parallel to the tip's shaft. In combination, successive measurements with differently angled tips might allow the systematic reconstruction of the entire complex electric field vector.

[1]B. Knoll and F. Keilmann, Opt. Commun. **182**(4–6), 321–328 (2000).
[2]R. Hillenbrand and F. Keilmann, Appl. Phys. B **73**, 239–243 (2001).
[3]R. Esteban, R. Vogelgesang, J. Dorfmüller, A. Dmitriev, C. Rockstuhl, C. Etrich, and K. Kern, Nano Lett. **8**(10), 3155–3159 (2008).

[4]A. Cvitkovic, N. Ocelic, and R. Hillenbrand, Opt. Express **15**(14), 8550–8565 (2007).
[5]E. Prodan, C. Radloff, N. J. Halas, and P. Nordlander, Science **302**(5644), 419–422 (2003).
[6]R. Vogelgesang, J. Dorfmüller, R. Esteban, R. T. Weitz, A. Dmitriev, and K. Kern, Phys. Status Solidi B **245**(10), 2255–2260 (2008).
[7]F. Hao, Y. Sonnefraud, P. Van Dorpe, S. A. Maier, N. J. Halas, and P. Nordlander, Nano Lett. **8**(11), 3983–3988 (2008).
[8]A. García-Etxarri, I. Romero, F. J. García de Abajo, R. Hillenbrand, and J. Aizpurua, Phys. Rev. B **79**(12), 125439 (2009).
[9]N. Verellen, Y. Sonnefraud, H. Sobhani, F. Hao, V. V. Moshchalkov, P. Van Dorpe, P. Nordlander, and S. A. Maier, Nano Lett. **9**(4), 1663–1667 (2009).
[10]R. Hillenbrand, F. Keilmann, P. Hanarp, D. S. Sutherland, and J. Aizpurua, Appl. Phys. Lett. **83**(2), 368–370 (2003).
[11]M. Rang, A. C. Jones, F. Zhou, Z.-Y. Li, B. J. Wiley, Y. N. Xia, and M. B. Raschke, Nano Lett. **8**(10), 3357–3363 (2008).
[12]M. Schnell, A. Garcia-Etxarri, J. Alkorta, J. Aizpurua, and R. Hillenbrand, Nano Lett **10**(9), 3524–3528 (2010).
[13]A. Bek, R. Vogelgesang, and K. Kern, Rev. Sci. Instrum. **77**(4), 043703 (2006).
[14]R. Esteban, R. Vogelgesang, and K. Kern, Nanotechnology **17**(2), 475–482 (2006).
[15]A. Bek, R. Vogelgesang, and K. Kern, Appl. Phys. Lett. **87**(16), 163115 (2005).
[16]R. Vogelgesang, R. Esteban, and K. Kern, J. Microsc. **229**(2), 365–370 (2008).
[17]E. O. Potma, W. P. de Boeij, and D. A. Wiersma, Biophys. J. **80**(6), 3019–3024 (2001).
[18]L. Gomez, R. Bachelot, A. Bouhelier, G. P. Wiederrecht, S.-H. Chang, S. K. Gray, F. Hua, S. Jeon, J. A. Rogers, M. E. Castro, S. Blaize, I. Stefanon, G. Lerondel, and P. Royer, J. Opt. Soc. Am. B **23**(5), 823–833 (2006).
[19]Y. Oshikane, S. Hara, T. Matsuda, H. Inoue, M. Nakano, and T. Kataoka, Surf. Interface Anal. **40**(6-7), 1054–1058 (2008).
[20]R. C. Dorf, *The Electrical Engineering Handbook* (CRC/Taylor & Francis, 2006).
[21]J. Dorfmüller, Ph.D. dissertation, EPFL, 2010.
[22]D. J. Schroeder, *Astronomical Optics*, 2nd ed. (Academic, San Diego, 2000).
[23]R. Loudon, 3rd ed. (Oxford University Press, Oxford, New York, 2000).
[24]R. Hillenbrand and F. Keilmann, Phys. Rev. Lett. **85**(14), 3029–3032 (2000).
[25]B. Deutsch, R. Hillenbrand, and L. Novotny, Opt. Express **16**(2), 494–501 (2008).
[26]N. Ocelic, A. J. Huber, and R. Hillenbrand, Appl. Phys. Lett. **89**(10), 101124 (2006).
[27]T. Zentgraf, J. Dorfmüller, C. Rockstuhl, C. Etrich, R. Vogelgesang, K. Kern, T. Pertsch, F. Lederer, and H. Giessen, Opt. Lett. **33**(8), 848–850 (2008).
[28]J. Dorfmüller, R. Vogelgesang, R. T. Weitz, C. Rockstuhl, C. Etrich, T. Pertsch, F. Lederer, and K. Kern, Nano Lett. **9**(6), 2372–2377 (2009).
[29]L. Novotny, R. X. Bian, and X. S. Xie, Phys. Rev. Lett. **79**(4), 645–648 (1997).
[30]T. Kalkbrenner, M. Ramstein, J. Mlynek, and V. Sandoghdar, J. Microscopy **202**(1), 72–76 (2001).
[31]Z. H. Kim and S. R. Leone, J. Phys. Chem. B **110**(40), 19804–19809 (2006).
[32]R. Esteban, R. Vogelgesang, and K. Kern, Phys. Rev. B **75**(19), 195410 (2007).
[33]S. C. Schneider, S. Grafström, and L. M. Eng, Phys. Rev. B **71**(11), 115418 (2005).